Applied Surface Science 313 (2014) 784–793

Contents lists available at ScienceDirect

Applied Surface Science

journal homepage: www.elsevier.com/locate/apsusc

Density functional theory study of water interactions on Mn-doped CeO_2(1 1 1) surface

Delfina García Pintos [a], Alfredo Juan [b], Beatriz Irigoyen [a,*]

[a] Departamento de Ingeniería Química, Facultad de Ingeniería, Universidad de Buenos Aires, Pabellón de Industrias, Ciudad Universitaria, 1428 Capital Federal, Argentina
[b] Departamento de Física and IFISUR, Universidad Nacional del Sur-CONICET, Avda. Alem 1253, 8000 Bahía Blanca, Argentina

ARTICLE INFO

Article history:
Received 13 April 2014
Received in revised form 10 June 2014
Accepted 11 June 2014
Available online 18 June 2014

Keywords:
Water adsorption
Mn-doped CeO_2(1 1 1) surface
Ceria
DFT + *U* calculations

ABSTRACT

Spin-polarized density functional theory (DFT + *U*) periodic calculations have been performed to study water adsorption and dissociation on the 12.5% Mn-doped CeO_2(1 1 1) surface. Our results indicated that Mn cation is the surface active site for water adsorption and dissociation reactions. The H_2O molecule preferably adsorbs on a Mn cation, causing some relaxation of the surface O-layer and, thus, facilitating the bonding of one of the H_{H_2O} with the nearest oxygen atom. After overcoming an energy barrier of 0.46 eV, the water molecule could dissociate into OH and H species. The latter configuration is about 50% more exothermic than the molecular one, suggesting the $Ce_{0.875}Mn_{0.125}O_{1.9375}$(1 1 1) surface would be easily hydroxylated under reaction conditions. In addition, the calculations showed that water adsorption on the Mn-doped CeO_2(1 1 1) surface did not favor the creation of surface oxygen vacancies as it has been reported for pure CeO_2(1 1 1). On the other hand, we created a surface oxygen defect in the slab with structural oxygen vacancies and computed water interactions on the reduced surface. Although, the adsorption of OH species in the O-hole caused many surface and subsurface atomic displacements, no changes in the oxidation state of Mn and Ce cations were detected.

1. Introduction

CeO_2-based solids have numerous technological applications, mainly due to the important oxygen storage capacity (OSC) of cerium oxide (ceria) [1]. These solids, with a fluorite-type structure, are extensively used as catalyst supports as well as active phases [1–4]. The catalytic performance of CeO_2-based materials has mainly been connected with the ability of ceria to undergo fast reversible redox cycles ($Ce^{4+} \rightarrow Ce^{3+}$), which accompany the release or uptake of oxygen [5,6].

Oxygen storage capacity, formation of Ce^{4+}/Ce^{3+} couples and oxygen mobility of ceria have been improved with the addition of late transition, alkaline or rare-earth metals [2,7]. Usually, transition metals (TM) exhibit several oxidation states and better redox properties than rare-earth metals [8]. Therefore, TM incorporation into the fluorite-type structure of CeO_2 facilitated the formation of oxygen vacancies and resulted in catalysts with enhanced OSC and improved redox properties [7,9,10].

Particularly, Mn-doped CeO_2 materials have shown excellent OSC and catalytic performance in many valuable oxygen-consuming processes [8–19]. The high activity of MnO_x–CeO_2 catalysts was ascribed to the synergistic interaction between MnO_x and CeO_2 [12]. MnO_x–CeO_2 mixed oxides were used as catalysts in many environmental processes: oxidation of diesel soot, ethanol, formaldehyde and phenol [8,13,14], selective reduction of NO with NH_3 [11], and oxidation of small hydrocarbon molecules and CO [15–19]. Mn dopant has also been considered a good candidate to take part of the CeO_2-based catalysts employed in the water-gas shift (WGS) reaction [20–22], which is of paramount importance for production of CO-free hydrogen [1].

In many of the previously discussed applications, water adsorption has been advised as an unavoidable process due to the presence of water either as a reactant or spectator [23]. Industrially, the adsorption of water is considered as an elementary step of the WGS reaction [1]. Moreover, in the case of phenol oxidation, it has been reported that hydroxyl species played a predominant role in the first step of phenol adsorption-oxidation reaction [24]. Therefore, water is impossible to exclude from realistic environments and this fact has raised the importance of understanding water interactions with CeO_2-based surfaces [25].

* Corresponding author. Tel.: +54 11 45763241; fax: +54 11 45763241.
E-mail address: beatriz@di.fcen.uba.ar (B. Irigoyen).

http://dx.doi.org/10.1016/j.apsusc.2014.06.076
0169-4332/

Several works have investigated water interactions on the CeO_2(1 1 1) surface performing ab-initio calculations [23,25–33]. Some of these studies reported that H_2O molecule could adsorb on the stoichiometric surface, through single H—$O_{surface}$ bond configuration [26,33], or forming two H—$O_{surface}$ bonds [28,31]. The adhesion of water molecule to CeO_2(1 1 1) surface has also been reported from experimental measurements [34]. Other theoretical works concluded that dissociative adsorption of water is energetically favored on the ideal surface [27], or that both molecular adsorption (no H-bond configuration) and dissociative adsorption (surface hydroxyl) states are possible on the slightly reduced CeO_2(1 1 1) surface [33]. Dissociative adsorption of water has also been evaluated through experimental measurements [35–39]. Both reduced CeO_{2-x} surfaces and CeO_2(1 1 1) films promoted dissociation of H_2O on the ceria substrate [36–39]. Besides, theoretical and experimental works suggested the filling of surface O-vacancies by hydroxyl groups [28,33,34]. On the other hand, X-ray photoelectron spectroscopy (XPS) and temperature-programmed desorption (TPD) measurements indicated the absence of irreversible water decomposition on reduced CeO_2(1 1 1) films grown on yttria-stabilized ZrO_2(1 1 1) [35].

Water interaction with a particular oxide is strongly dependent on the surface structure (presence, accessibility, and coordination of metal cations) [40]. In that sense, we underline that MnO_x–CeO_2 mixed oxides expose surface Mn and also Ce cations with a different O-coordination environment than that of pure CeO_2. Besides, despite the extensive research effort dedicated to understand water behavior on CeO_2, to the best of our knowledge, no research studies of H_2O interactions on MnO_x–CeO_2 catalysts are available. Therefore, in this work, we performed density functional (DFT + U) calculations to characterize molecular and dissociative adsorption of water on the Mn-doped CeO_2(1 1 1) surface.

2. Theoretical method

2.1. Calculation details

All spin polarized calculations were carried out using the Vienna Ab-initio Simulation Package (VASP) [41,42].

The Kohn–Sham equations were solved with the generalized gradient approximation (GGA) using the exchange-correlation functional of Perdew–Burke–Ernzerhof (PBE) [43]. The core electrons were represented with the projector augmented wave (PAW) method [44]. The valence electron wave functions were expanded using a truncation energy value of 408 eV, and a Gaussian smearing of 0.2 eV. We used the valence configurations $5s^2$, $5p^6$, $6s^2$, $5d^1$, $4f^1$ for Ce; $3d^6$, $4s^1$ for Mn; $2s^2$, $2p^4$ for O, and $1s^1$ for H. The Brillouin zone was sampled with a $3 \times 2 \times 1$ k-points grid according to the Monkhorst–Pack scheme [45]. Structural relaxations were performed according to the Hellmann–Feynman approximation and the atomic positions were relaxed until the force acting on each atom was smaller than 0.02 eV/Å. For the energy calculations we considered spin polarization effects.

We also checked the possible effects of surface dipoles on the energetics of both water adsorption and oxygen vacancies formation on the $Ce_{0.875}Mn_{0.125}O_{1.9375}$(1 1 1) surface, by adding a compensating electric field as implemented in the VASP code. The calculations were affected in less than 0.01 eV, and thus, dipole correction was not included in the results reported in the present work.

The standard DFT formulation usually fails to describe strongly correlated electrons due to a deficient treatment of electron correlation. This limitation has been corrected to some extent by using the DFT + U method, where the introduction of a Hubbard parameter U modified the self-interaction error and enhanced the description of the correlation effects [46,47]. Recently, the performance of a precise van der Waals density functional (vdW-DF) approach has been tested for a range of solids, showing that some of the modified vdW functionals lead to average errors which are similar to those of PBE, while atomization energies are slightly better than those from PBE [48]. According to our previous study [49], in the present work we used the Hubbard parameter: $U = 5$ eV for Ce(4f) states, and $U = 4.5$ eV for Mn(3d) orbitals. The U value of 5 eV was chosen for the Ce(4f) states as it correctly described the atomic and electronic structure of both CeO_2 and CeO_{2-x} systems [7,50–54]. On the other hand, a value of $U = 4.5$ eV was reliable for the description of the strong on-site Coulomb repulsion among Mn(3d) electrons [55,56]. The selected value has shown to be reasonable, reproducing the experimentally available data for MnO such as lattice constant, band gap and Mn—O bond lengths [56].

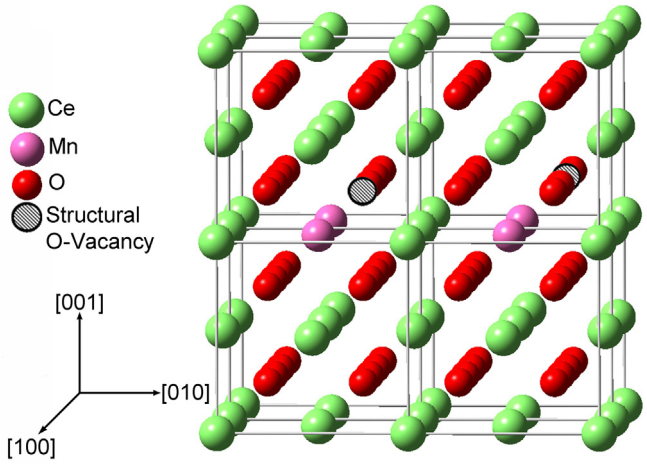

Fig. 1. $Ce_{0.875}Mn_{0.125}O_{1.9375}$ bulk supercell.

2.2. Model of the 12.5% Mn-doped CeO_2 bulk and (1 1 1) surface

The cerium oxide (CeO_2) has a fluorite-type structure with a lattice parameter value of 5.4113 Å (JCPDS 43-1002), and can form solid solutions when doped with Mn [9,11,12]. The reported limit for MnO_x solubility in CeO_2 was about 15% Mn cationic content (i.e. Mn/(Ce + Mn) < 0.15) [13,57]. Besides, for a 10% Mn mixing into CeO_2, it was observed a slight decrease in the lattice parameter value (5.406 Å [8], 5.408 Å [11], 5.4108 Å [58]).

Starting from the stoichiometric supercell, formed by 32 cations and 64 oxygen anions, we introduced the four Mn dopant cations as two pairs of second nearest-neighbors of Ce cations (see Fig. 1).

For the resulting $Ce_{0.875}Mn_{0.125}O_2$ supercell, we calculated an optimized lattice constant value of 5.463 Å [49]. Therefore, the doping of CeO_2 with 12.5% of Mn resulted in a reduction of its lattice parameter, from 5.49 to 5.463 Å, in good agreement with reported experimental data noticing a small lattice parameter shrinkage for MnO_x–CeO_2 solid solutions [8,11]. In addition, we observed distortions in Ce-O bond lengths, which changed from 2.37 Å in pure CeO_2 to values in the 2.36–2.38 Å range. After that, we removed two bulk oxygen atoms from the $Ce_{0.875}Mn_{0.125}O_2$ supercell (see Fig. 1), because experimental studies indicated that MnO_x–CeO_2 solid solutions present structural O-vacancies [8,11,13,57,10]. The calculations gave a negative value for these O-vacancies formation energy ($\Delta E_{Bulk\ 2O\text{-}vac.} = -2.23$ eV), indicating a more stable O-deficient 12.5% Mn-doped CeO_2 fluorite-type bulk structure with a $Ce_{0.875}Mn_{0.125}O_{1.9375}$ composition.

For the study of H_2O interactions on the 12.5% Mn-doped CeO_2 catalyst, we considered the (1 1 1) surface terminated with an extra O-layer. Considering the scarce experimental data related to

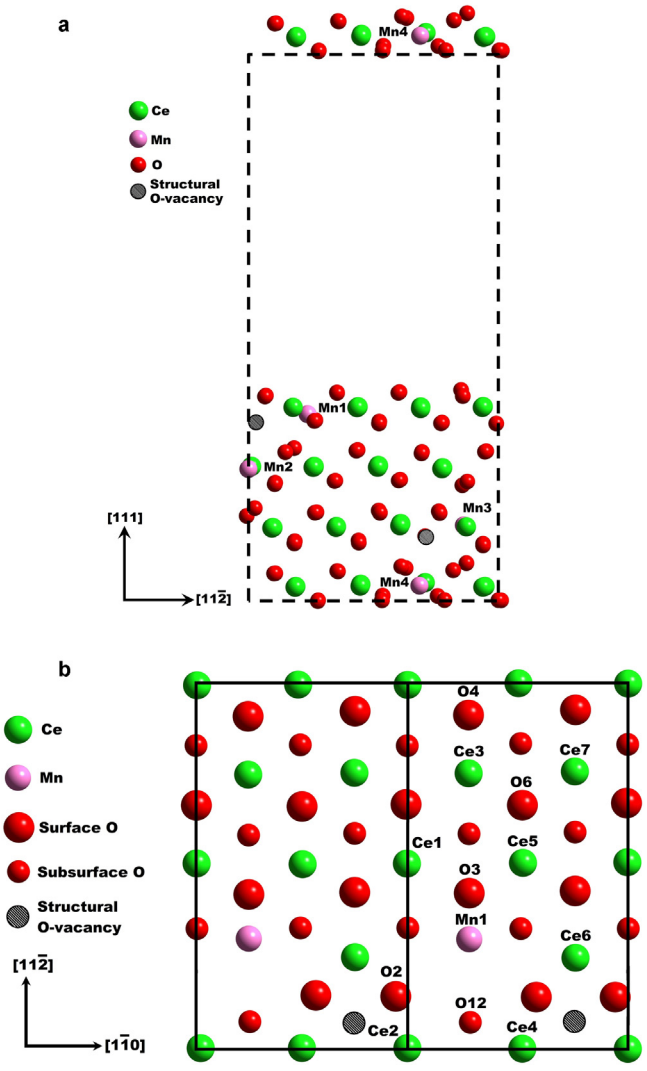

Fig. 2. The structural-oxygen-deficient $Ce_{0.875}Mn_{0.125}O_{1.9375}(1\,1\,1)$ slab. (a) Top view, (b) side view. Different Ce cations and O anions are labeled.

relative stability of the low-index faces of MnO_x–CeO_2 mixed oxides, our (1 1 1) structural assignment was based on that of pure CeO_2 [59–62]. In that sense, DFT calculations performed on well defined CeO_2 surfaces, using both GGA + U and B3LYP exchange-correlation functionals, consistently predicted that $CeO_2(1\,1\,1)$ is the most stable low-index surface [59]. This theoretical finding agrees with experimental results reported from X-ray photoemission spectroscopy (XPS) and low-energy electron-diffraction (LEED) measurements, which demonstrated the higher stability of the $CeO_2(1\,1\,1)$ surface [59]. Besides, oxygen-terminated $CeO_2(1\,1\,1)$ surfaces were visualized by noncontact atomic force microscopy (NC-AFM) [61]. Accordingly, theoretical ab-initio thermodynamics calculations showed that, under oxygen-rich conditions, the most stable surface structure of CeO_2 is the stoichiometric (1 1 1) surface; while, for a highly reducing environment, the (1 1 1) Ce-terminated surface becomes energetically favored [62].

In the present calculations, we employed the same model for the $Ce_{0.875}Mn_{0.125}O_{1.9375}(1\,1\,1)$ surface as in our previous work [49]; a stack of O-cations-O sandwiches, which prevents the appearance of a nonzero dipole moment normal to the surface [63]. This surface was modeled with a slab formed by twelve atomic layers, two structural oxygen vacancies and a vacuum space of 20 Å (see Fig. 2a). The latter avoids periodic interactions with the atoms of the upper image. For all energy calculations we allowed the adsorbate (H_2O or OH and H species), and Ce, Mn and O ions located in the six uppermost layers of the slab to fully relax, while keeping fixed the atomic positions of the ions at the six lowermost layers.

The structural-oxygen-deficient $Ce_{0.875}Mn_{0.125}O_{1.9375}(1\,1\,1)$ slab exposes surface Ce cations with different environments and also a Mn cation. In Fig. 2b, we labeled some of these surface cations, including Ce2, Ce5, Ce6, Ce7 and Mn1, which were considered for studying water interactions. Note that Ce1 is similar to Ce5, Ce2 to Ce4 and Ce3 to Ce7. In addition, Ce2 and Ce4 are located near a structural O-vacancy, Ce1 and Ce5 are close to the Mn1 dopant, and Ce6 is neighbored by Mn1 and a structural O-vacancy.

For molecular and dissociative adsorption of water on the structural-oxygen-deficient $Ce_{0.875}Mn_{0.125}O_{1.9375}(1\,1\,1)$ surface, we calculated the adsorption energy as follows:

$$\Delta E_{ads,H_2O} = E_{[H_2O/Ce_{0.875}Mn_{0.125}O_{1.9375}(1\,1\,1)]} - E_{[Ce_{0.875}Mn_{0.125}O_{1.9375}(1\,1\,1)]} - E_{[H_2O]},$$

$$\Delta E_{ads,H-OH} = E_{[H-OH/Ce_{0.875}Mn_{0.125}O_{1.9375}(1\,1\,1)]} - E_{[Ce_{0.875}Mn_{0.125}O_{1.9375}(1\,1\,1)]} - E_{[H_2O]}$$

where $E_{[H_2O/Ce_{0.875}Mn_{0.125}O_{1.9375}(1\,1\,1)]}$ and $E_{[H-OH/Ce_{0.875}Mn_{0.125}O_{1.9375}(1\,1\,1)]}$ represent the total energy of the systems resulting from molecular and dissociative adsorption of water on the structural-oxygen-deficient $Ce_{0.875}Mn_{0.125}O_{1.9375}(1\,1\,1)$ surface, respectively. $E_{[Ce_{0.875}Mn_{0.125}O_{1.9375}(1\,1\,1)]}$ is the total energy of the structural-oxygen-deficient bare surface, while $E_{[H_2O]}$ represents the energy of a water molecule in the vacuum. A negative value of $\Delta E_{ads,H_2O}$ or $\Delta E_{ads,H-OH}$ means these interactions are exothermic.

3. Results and discussion

In the following we discuss the energetics of H_2O adsorption on the Mn-doped $CeO_2(1\,1\,1)$ surface. We studied molecular and dissociative adsorption of water on the structural-oxygen-deficient $Ce_{0.875}Mn_{0.125}O_{1.9375}(1\,1\,1)$ slab with and without surface oxygen vacancies.

3.1. Molecular adsorption of H_2O on the structural-oxygen-deficient $Ce_{0.875}Mn_{0.125}O_{1.9375}(1\,1\,1)$ slab

The computed energy values for molecular adsorption of H_2O on different surface Ce and Mn cations of the $Ce_{0.875}Mn_{0.125}O_{1.9375}(1\,1\,1)$ slab are reported in Table 1. Besides, the structural parameters for stable configurations of adsorbed H_2O molecule are shown in Table 1. The calculated energy values clearly indicate the interaction of water on the Mn dopant was most favorable than on Ce cations. In this concern, we underline the stability of water adsorption process related to different surface sites was: Mn (−0.81 eV) > Ce6 (−0.53 eV) > Ce5 (−0.50 eV) > Ce2 (−0.44 eV) > Ce7 (−0.39 eV).

Water chemisorbed on the Mn site ($\Delta E_{ads,H_2O} = -0.81$ eV), with a tilt angle of ~49°. Due to this interaction, the O_{H_2O} bonded to the Mn cation, while the hydrogen that pointed to the surface formed a bond with the nearest oxygen atom of the O-extra layer. The length of the O_{H_2O}-Mn bond resulted in 2.16 Å and that of the formed H—$O_{surface}$ bond in 1.46 Å (see Fig. 3a). Due to formation of the later bond, the corresponding $(O\text{-}H)_{H2O}$ bond enlarged up to 1.06 Å and the angle of H—O—H bonds resulted in 108.02° (see Table 1). Note that, after optimization of water molecule in vacuum, we calculated O-H bonds length of 0.97 Å and H—O—H angle of 104.55°. This interaction also reflected in relaxations of surface oxygen anions. In Fig. 3a, it can be seen that a surface oxygen anion was displaced 0.17 Å parallel to the (1 1 1) plane, toward the position of the water molecule. Besides, the oxygen placed near the H_2O molecule moved 0.18 Å outward the surface, while another oxygen descended 0.15 Å (see Fig. 3b).

Table 1
Water molecule interactions on different active sites of the structural-oxygen-deficient $Ce_{0.875}Mn_{0.125}O_{1.9375}$(1 1 1) slab. Adsorption energy and structural details.

Site	Neighbors	$\Delta E_{ads,H_2O}$ (eV)	d(O-cation) (Å)	d(O-H1) (Å)	d(O-H2) (Å)	H1-O-H2 (°)
Mn1		−0.81	2.16	0.97	1.06	108.02
Ce6	Structural O-defect, Mn dopant	−0.53	2.62	0.97	1.01	108.92
Ce5	Mn dopant	−0.50	2.63	0.97	1.01	108.16
Ce2	Structural O-defect	−0.44	2.70	0.97	1.00	106.58
Ce7		−0.39	2.61	0.97	0.99	111.80

As mentioned before, we found that interactions of water molecule on Ce2, Ce5, Ce6 and Ce7 cations were less stable than on Mn dopant. As it can be seen in Table 1, water physisorbed on Ce sites. Even considering the more favorable water interactions on Ce5 and Ce6 cations, which are located near a Mn dopant (see Fig. 2b), the computed adsorption energy values were −0.50 and −0.53 eV, respectively. Clearly, these two structures resulted to be very close in energy. The H_2O molecule bonded to the Ce6 cation by its oxygen, which located at 2.62 Å on top of Ce6. As a result, one of its hydrogen pointed out of the surface; while the another tilted toward the surface, finishing at 1.72 Å from the nearest $O_{surface}$. Consequently, the corresponding water H—O bond stretched about 4% (see Table 1: d(O–H_2) = 1.01 Å) and the H—O—H angle resulted in 108.92°. Concerning the interaction on Ce5 cation, we underline the H_2O molecule adopted a geometric configuration similar to that on Ce6; the O_{H_2O}-Ce5 and the H—$O_{surface}$ bond lengths were 2.63 Å and 1.69 Å, respectively. On the other hand, molecular interactions of water on Ce2 and Ce7, which are located far from a Mn dopant (see Fig. 2b), were weaker than adsorption on Mn. Due to water interaction on Ce2 ($\Delta E_{ads,H_2O} = -0.44\,eV$), the O_{H_2O} sited above the metal cation with the longer calculated distance (see Table 1: d(O-Ce2) = 2.70 Å), while the H_{H_2O} tilted downward and located at 1.78 Å distance from the nearest $O_{surface}$. Besides, the calculated adsorption energy value for water-Ce7 interaction resulted in -0.39 eV (see Table 1). The analysis of this configuration showed an O_{H_2O}-Ce7 distance of 2.61 Å, while the H—$O_{surface}$ distance (1.88 Å) resulted to be the longest one. We emphasize this process was the less stable among all those studied on the $Ce_{0.875}Mn_{0.125}O_{1.9375}$(1 1 1) surface. Even more, our calculated energy values for water molecule interactions on Ce sites are in agreement with those previously reported on pure CeO_2. In that sense, water interactions with Ce cations on the undoped CeO_2(1 1 1) surface have been previously assessed with DFT + U (U = 5 eV) approach and the PW91 exchange-correlation functional [27,29,31]. These works reported that H_2O physisorbed on the ideal CeO_2(1 1 1) surface with energy values of −0.36 eV [27], −0.51 eV [29], or −0.49 eV [31]. The presence of step sites moderately affected the molecular interaction of water, which adsorbed on the CeO_2(3 3 1) surface with an adsorption energy value of −0.72 eV [32]. From calculations with a PBE + U (U = 5 eV) approach, water adsorption energy values of −0.54 eV [25] and −0.57 eV [30], have been reported on the CeO_2(1 1 1) surface. In addition, the negligible coverage dependence for adsorbed water on the stoichiometric (1 1 1) surface was ascribed to a lack of interactions among adsorbed H_2O molecules [23]. On the other hand, a combined experimental and theoretical study indicated that water adsorption at both the terrace ($\Delta E_{ad(H_2O)} = -0.50$ eV) and step ($\Delta E_{ad(H_2O)} = -0.89$ eV) sites of CeO_2(1 1 1) surface are favorable [39].

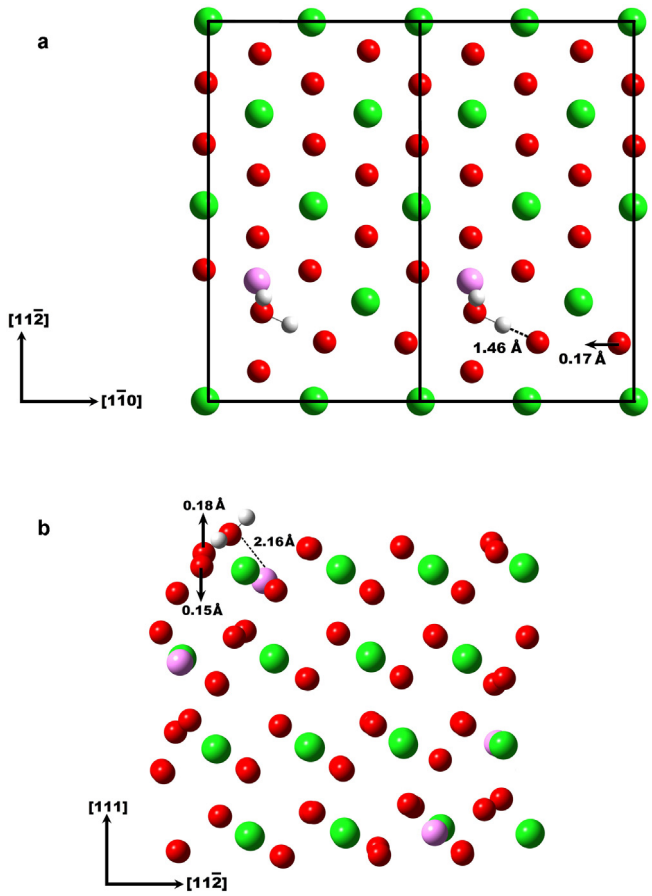

Fig. 3. Preferential molecular adsorption of water on the structural-oxygen-deficient $Ce_{0.875}Mn_{0.125}O_{1.9375}$(1 1 1) slab. (a) Top view, (b) side view.

Furthermore, in the present work we also studied the electronic effects of molecular water interactions on the structural O-deficient $Ce_{0.875}Mn_{0.125}O_{1.9375}$(1 1 1) surface. Therefore, in order to evaluate the oxidation state of Mn and Ce cations, we performed Bader charge and spin-magnetization analyses [64]. The electronic structure of CeO_2, when treated with the PAW approximation, has been reported as tetravalent Ce cations with an unoccupied Ce(4f) band ($4f^0$) and a completely filled O(2p) valence band [50]. In this approach, the reduction of a Ce cation was originated by one electron being localized in Ce(4f) band ($4f^1$), in accordance with UPS/XPS experimental data [65]. Accordingly, Bader charge analysis always assigns 9.6 electrons to Ce^{4+} and 9.9 electrons to Ce^{3+} cations.

On the other hand, the oxidation state of Mn cation could best be determined by integrating the spin-polarization density due to Mn is a high-spin transition metal [66]. This procedure, in comparison with integrating charge density, allowed to filter out the O(2p) contributions. Considering Bader charge analysis of the spin-polarization density, it is worthy to note the process of $Ce^{4+} \rightarrow Ce^{3+}$ reduction results in a change from 0 μ_B to 1 μ_B. However, the assignment of Mn oxidation states in the $Ce_{0.875}Mn_{0.125}O_{1.9375}$(1 1 1) surface is more complex as it was extensively discussed in our previous work [49]. The spin magnetization of Mn1, Mn2, Mn3 and Mn4 cations (see Fig. 2a, for identification of these cations) was calculated therein as 4 μ_B, 4.16 μ_B, 4.15 μ_B and 4.13 μ_B, respectively; while that of Ce cations resulted in 0 μ_B. Meanwhile, the DOS curve showed several localized unoccupied gap states associated to the contribution of both

Mn(3d)-O(2p) states and Ce(4f) orbitals. From these results, we concluded that Mn and Ce would be as Mn^{3+} and Ce^{4+} ions in the clean $Ce_{0.875}Mn_{0.125}O_{1.9375}$(1 1 1) surface [49]. Accordingly, charge calculations performed in the present work indicated the oxidation state of Mn dopants and that of surface and inner Ce cations remained unaltered as Mn^{3+} and Ce^{4+}, after water adsorption on top of Mn or Ce cations. Therefore, we underline that our results did not show neither $Mn^{3+} \rightarrow Mn^{2+}$ nor $Ce^{4+} \rightarrow Ce^{3+}$ reduction due to molecular adsorption of H_2O.

3.2. Dissociative adsorption of water on the structural-oxygen-deficient $Ce_{0.875}Mn_{0.125}O_{1.9375}$(1 1 1) slab with and without surface oxygen vacancies

In this section, we discuss the structure and energetics of the dissociative adsorption of water (OH and H species) on the $Ce_{0.875}Mn_{0.125}O_{1.9375}$(1 1 1) surface.

3.2.1. OH and H species adsorption on the $Ce_{0.875}Mn_{0.125}O_{1.9375}$(1 1 1) slab without surface oxygen vacancies

The computed energy values for the dissociative adsorption of water (OH and H species) on different surface sites of the structural-oxygen-deficient $Ce_{0.875}Mn_{0.125}O_{1.9375}$(1 1 1) slab are reported in Table 2. The structural parameters for the corresponding stable configurations are also shown in Table 2. As it can be seen, all optimized configurations led to OH fragment bonded to a surface cation, while the H species bonded to oxygen anions.

Our results indicate that OH and H species could adsorb on metal cation and $O_{surface}$ sites, respectively, with calculated adsorption energy values of: −1.21 eV (Mn) > −0.67 eV (Ce6) > −0.50 eV (Ce5) > −0.38 eV (Ce2) > −0.27 eV (Ce7). These dissociated water structures followed the same stability trend that molecular water configurations. The most exothermic interaction resulted from binding of the OH and H species to a Mn cation and to an oxygen anion coordinated with Ce cations (O_{Ce}), respectively. The computed energy value ($\Delta E_{ads,OHH} = -1.21$ eV) implicates that water underwent strong dissociative chemisorption on Mn dopant at the $Ce_{0.875}Mn_{0.125}O_{1.9375}$(1 1 1) surface. The calculated O_{OH}–Mn distance resulted in 1.89 Å, which is similar to the length computed for the Mn–O bonds on the bare surface (in the range of 1.91–1.95 Å). The OH species bonded to Mn tilted downward, forming a H—O—Mn angle of 103.51°. In addition, the H species was attracted to the adjacent O_{Ce} cation forming a H—O_{Ce} bond of 1.01 Å length.

On the other hand, the calculated adsorption energy values for the dissociative interaction of water on Ce2, Ce5, Ce6 and Ce7 sites ranged from -0.27 to -0.67 eV. Overall, the analysis of the optimized structures showed that lengths of O_{OH}–Ce bond ranged between 2.18 Å and 2.31 Å (see Table 2: $d(O_{OH}–Ce2) = 2.18$ Å, $d(O_{OH}–Ce6) = 2.31$ Å), while the computed values for H—$O_{surface}$ bond distances ranged from 0.98 Å (Ce2) to 1.04 Å (Ce6). The calculated O_{OH}–Ce distances resulted to be shorter than those calculated for O-Ce bonds in the bare $Ce_{0.875}Mn_{0.125}O_{1.9375}$(1 1 1) surface (in the range of 2.30 Å - 2.43 Å). Moreover, we underline the interactions of lower binding energy corresponded to those of OH species on Ce7 ($\Delta E_{ads,OH–H} = -0.27$ eV) and Ce2 ($\Delta E_{ads,OH–H} = -0.38$ eV) cations, which are located far from a Mn dopant, with the hydrogen species bonded to the nearest surface oxygen anion. These interactions were also less favorable than those of H_2O molecule on Ce2 and Ce7 sites (13.6% and 30%, respectively). We also note the obtained dissociative geometries exhibit the OH species mainly tilted toward surface Ce cations, forming H—O—Ce2 and H—O—Ce7 angles of 127.39° and 134.78°, respectively. However, the adsorption on Ce5 cation, which is located near Mn1 (see Fig. 2b), was more favorable ($\Delta E_{ads,OH–H} = -0.50$ eV), although no energy difference was found between both dissociated and molecular interactions. On the other hand, an adsorption energy value $\Delta E_{ads,OH–H} = -0.67$ eV was obtained when the OH species interacted on the Ce6 site, which is neighboring by Mn1 and a structural O-defect (see Fig. 2b). Noticeably, the calculated energy value for dissociative interaction of water on Ce6 is about 55% of that computed on Mn dopant. The dissociative geometry shows the OH species tilted toward the surface, forming a H–O–Mn angle of 137.45°, with the H species bonded to the nearest O_{Ce} anion (see Table 2: $d(H—O_{Ce}) = 1.04$ Å). Our computed values on Ce sites are in agreement with the reported energetic for the dissociative adsorption of water (−0.59 eV) on the stoichiometric CeO_2(1 1 1) surface [23]. On the oxidized CeO_2(1 1 1) surface, the calculated energy values for dissociative interaction of water were −0.59 eV [23], and −0.66 eV [27]. The OH group became adsorbed at 2.22 Å above a Ce cation, while the H bonded to the adjacent surface O anion forming a H—O_{Ce} bond of 1.65 Å length and stretching the corresponding O–Ce distance to 3.00 Å [23]. Besides, H_2O dissociative adsorption was favored by its interaction on the stepped surface of ceria (-1.21 eV) [39]. Recently, water interactions on Ce cations of the CeO_2(1 1 1) surface have been evaluated considering van der Waals interactions and different approximations to exchange and correlation functionals, predicting similar energies (∼ 0.7 eV) for the molecular structure with one H—$O_{surface}$ bond and the hydroxyl pair [25]. On the other hand, experimental studies on fully oxidized CeO_2(1 1 1) thin films showed that hydroxyls could adsorb atop Ce cations; but these hydroxyls recombined and desorbed between 200 and 300 K [40].

With regard to the most stable configuration of dissociatively adsorbed water on the $Ce_{0.875}Mn_{0.125}O_{1.9375}$(1 1 1) surface, we highlight that binding of OH and H species to Mn dopant and O_{Ce} anions, respectively, reflected in important atomic displacements. As can be seen in Fig. 4a, the Mn dopant itself moved 0.78 Å, acquiring a similar arrangement to that of its neighboring Ce cations. Meanwhile, the surface O_{Ce} anion that bonded to hydrogen relaxed 0.48 Å in the same direction. Among all observed atomic movements in the direction of the normal (see Fig. 4b), the more noticeable displacements were those of an oxygen coordinated with Ce cations and bonded to H, which ascended 0.47 Å, and a Mn cation located at an inner layer of the slab, which descended 0.23 Å.

Finally, in order to quantify the effect of the van der Waals (vdW) dispersion forces during water interactions, and detect whether these forces could improve the stability of both molecular and dissociative states, we performed calculations taking vdW forces into account as implemented in the DFT-D2 method [67]. With this correction, we found differences of approximately 0.001 and 0.06 eV for molecular and hydroxyls configurations, respectively. These results suggested that vdW dispersion forces have very little influence in water interactions on the 12.5% Mn-doped CeO_2(1 1 1) surface. Moreover, the only detected structural difference was that of the formed H—$O_{surface}$ bond which length enlarged 0.01 Å (less than 0.5%) when considering wdW corrections. Therefore, vdW dispersion forces were not further considered in our calculations.

3.2.2. OH and H species adsorption on the $Ce_{0.875}Mn_{0.125}O_{1.9375}$(1 1 1) slab with a surface oxygen vacancy

We also studied the dissociative interaction of H_2O on the Mn-doped CeO_2 system with a surface oxygen vacancy. In a previous paper [49], we computed the formation of surface oxygen vacancies on the structural-oxygen-deficient $Ce_{0.875}Mn_{0.125}O_{1.9375}$(1 1 1) slab. The considered oxygen anions have different neighboring cations and were labeled as O2, O3 and O4 (see Fig. 2b). The oxygen O2 is near a structural O-vacancy. The oxygen O3 coordinates with Mn and Ce cations, while the oxygen O4 is bonded to Ce cations and is relatively far from a Mn dopant or structural O-defect. We calculated the energy required for surface O2-, O3- and O4-vacancy

Table 2
Dissociated water adsorption on different active sites of the structural-oxygen-deficient $Ce_{0.875}Mn_{0.125}O_{1.9375}(111)$ slab. Adsorption energy and structural details.

Site	Neighbors	$\Delta E_{ads,OH-H}$ (eV)	d(O-cation) (Å)	$d(O\text{-}H1)_{OH}$ (Å)	$d(O_{surf}\text{-}H2)$ (Å)
Mn1		−1.21	1.89	0.98	1.01
Ce6	Structural O-defect, Mn dopant	−0.67	2.31	1.00	1.04
Ce5	Mn dopant	−0.50	2.22	0.97	1.01
Ce2	Structural O-defect	−0.38	2.18	0.96	0.98
Ce7		−0.27	2.23	0.97	1.02

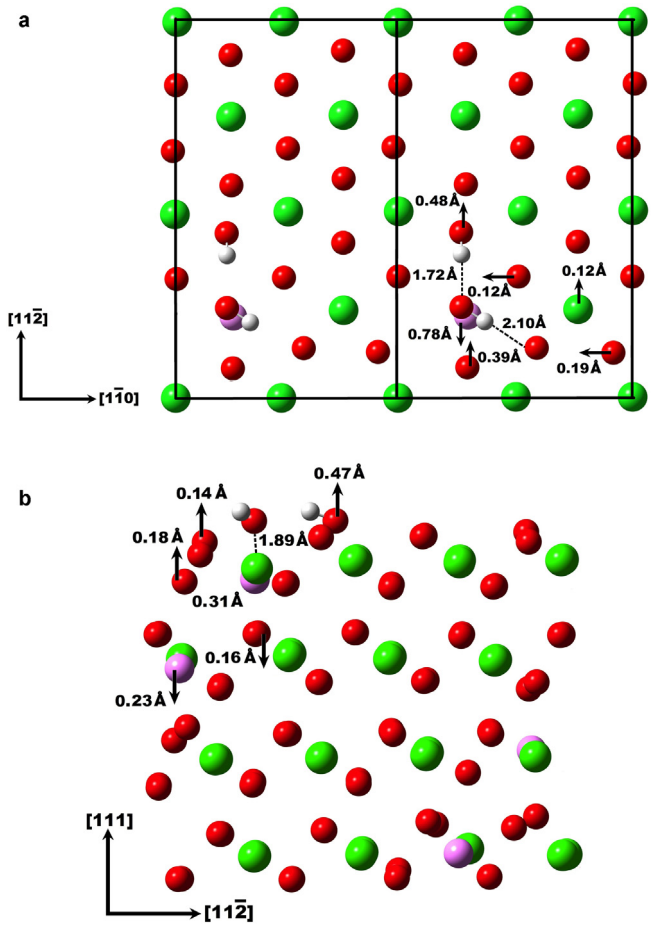

Fig. 4. Dissociative adsorption of water on the structural-oxygen-deficient $Ce_{0.875}Mn_{0.125}O_{1.9375}(1\,1\,1)$ slab. (a) Top view, (b) side view.

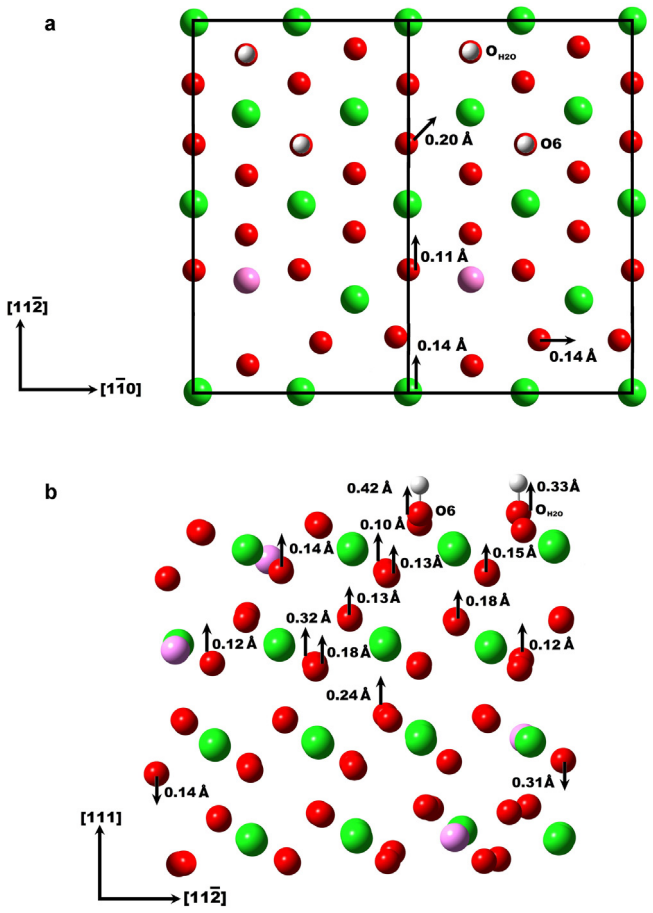

Fig. 5. Dissociative adsorption of water on the structural-oxygen-deficient $Ce_{0.875}Mn_{0.125}O_{1.9375}(1\,1\,1)$ slab with a surface oxygen vacancy. (a) Top view, (b) side view.

formation as these anions represent different oxygen sites of the 12.5% Mn-doped $CeO_2(1\,1\,1)$ surface.

The computed energy values for surface O4-, O3- and O2-vacancy creation were 0.38, 0.66, and 0.77 eV, respectively [49]. Due to the removal of O4 from the surface, the Mn2 and Mn3 cations became reduced and adopted the (2+) oxidation state [49]. Besides, the density of states (DOS) curve showed the occupied Mn2(3d)–O(2p) and Mn3(3d)–O(2p) states on and below the Fermi level (see supplementary information in Ref. [49]), indicating that the electron density left behind by O4 removal was transferred to Mn2 and Mn3 cations.

Therefore, we evaluated the dissociative adsorption of water on the structural-oxygen-deficient $Ce_{0.875}Mn_{0.125}O_{1.9375}(1\,1\,1)$ slab with the surface O4-vacancy. The computed adsorption energy for this interaction is $\Delta E_{ads,H-OH} = -0.69$ eV. The calculations showed the OH species adsorbed, through its oxygen, in the hole left by surface O4-vacancy formation (O4-hole), while the H bonded to the oxygen O6 (see Fig. 5a and b). The distance from the hydroxyl oxygen (O_{OH}) to the original O4 position is 0.33 Å. Due to the OH species adsorption on the O4-hole, the O_{OH} coordinated to three Ce cations. The resulting O_{OH}–Ce distances are 2.57 Å (2) and 2.58 Å. Note that, on the bare Mn-doped $CeO_2(1\,1\,1)$ surface, the length of O4-Ce bonds are 2.30 Å and 2.34 Å (2). The H_{H_2O} adsorbed on the oxygen O6 and the length of the formed H_{H_2O}-O_6 bond is 0.97 Å. The O6-Ce bonds were enlarged to 2.58, 2.61 and 2.66 Å (2.30 Å (1) and 2.34 Å (2), in the bare surface). Consequently, many surface and subsurface atomic displacements were detected. Moreover, the two hydroxyl species (H_{H_2O}-O_6 and $(H{-}O)_{H2O}$) drained the corresponding oxygen anions outward the surface by 0.42 and 0.33 Å (see Fig. 5b).

Our findings about dissociative interaction of water on the structural-oxygen-deficient $Ce_{0.875}Mn_{0.125}O_{1.9375}(1\,1\,1)$ slab with the surface O4-vacancy ($\Delta E_{ads,H-OH} = -0.69$ eV), are in agreement with both theoretical [23,27–29,33], and experimental studies [34,35,37,40], which indicated that H_2O could dissociate on the reduced $CeO_2(1\,1\,1)$ surface. Also, it was reported that formed OH groups are able to fill the surface oxygen vacancies [27,28,33]. On the reduced $CeO_{2-x}(1\,1\,1)$ thin films, water could adsorb and dissociate on the 3-fold Ce sites; but most of these hydroxyls reacted

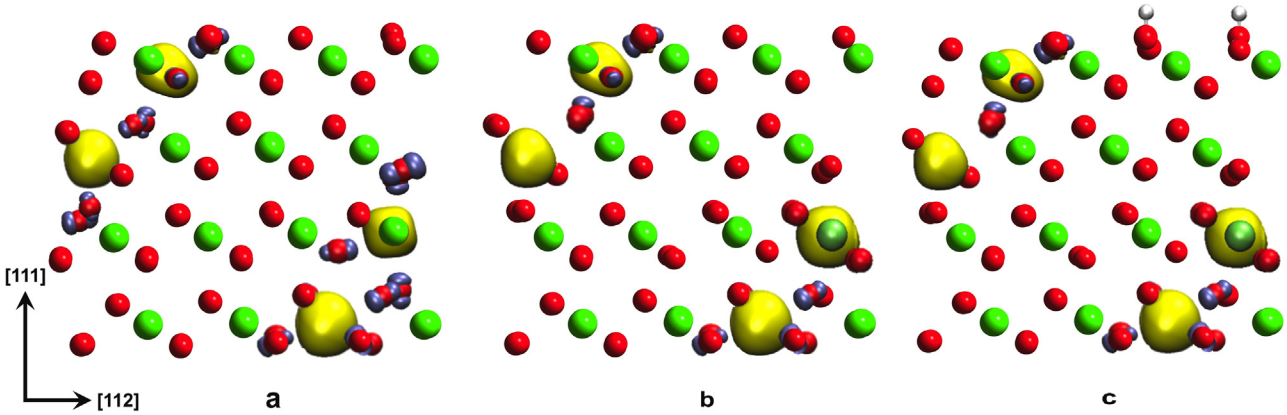

Fig. 6. Spin polarization surfaces at a 0.05 e Å^{-3} isovalue (side view) for different structural-oxygen-deficient $Ce_{0.875}Mn_{0.125}O_{1.9375}$(1 1 1) systems. Positive and negative values are indicated in yellow and gray, respectively. (a) The bare $Ce_{0.875}Mn_{0.125}O_{1.9375}$(1 1 1) surface. All Mn cations are present in (3+) oxidation state. (b) The $Ce_{0.875}Mn_{0.125}O_{1.9375}$(1 1 1) surface without O4. Mn2 and Mn3 are as Mn^{2+}, while Mn1 and Mn4 remain in (3+) oxidation state. (c) The $Ce_{0.875}Mn_{0.125}O_{1.9375}$(1 1 1) surface without O4, interacting with OH and H species. Mn2 and Mn3 remain as (2+).

at 560 K, producing H_2 and leaving oxygen on the surface [40]. In contrast, the dissociation of water on reduced CeO_2 was found to be fully reversible yielding H_2O (by recombination of the OH groups) or releasing hydrogen and oxygen into the gas phase [39].

Finally, in order to evaluate the possibility of surface reoxidation, we performed Bader charge and spin-magnetization analyses. The results of the spin-polarized charge density for different structural-oxygen-deficient 12.5% Mn-doped CeO_2(1 1 1) slabs, can be seen in Table 3. The corresponding spin-polarization surfaces, at a 0.05 e Å^{-3} isovalue, are shown in Fig. 6. Related to the $Ce_{0.875}Mn_{0.125}O_{1.9375}$(1 1 1) system without surface O-defects, as previously discussed, the spin magnetization of Mn1, Mn2, Mn3 and Mn4 cations was calculated in 4 μ_B, 4.16 μ_B, 4.15 μ_B and 4.13 μ_B, respectively, while that of Ce cations in 0 μ_B. Accordingly, the spin-polarization surface of the substrate without surface O-vacancies shows the four Mn cations of the slab in the (3+) oxidation state and the Ce cations in (4+) (see Fig. 6a). On the other hand, Fig. 6b shows the spin-polarization curves of the substrate when the O4-vacancy was formed, which led to the reduction of two Mn^{3+} cations to Mn^{2+} (see Mn2 and Mn3) as it was discussed in Ref. [49]. Finally, Fig. 6c shows the spin-polarization curves of the substrate with the O4-vacancy and a dissociated H_2O molecule, with the OH fragment replenishing the O4-hole and the remaining H species interacting with a surface oxygen anion (O6, as labeled in Fig. 2b). In this last picture, it can be observed that Mn cations have the same oxidation states as those of Fig. 6b, despite OH replenishing the O4-hole. Therefore, our results indicate that dissociative adsorption of water on the $Ce_{0.875}Mn_{0.125}O_{1.9375}$(1 1 1) slab with a surface oxygen vacancy did not reoxidize the Mn^{2+} cations (Mn2 and Mn3), which were previously reduced due to the O4-vacancy formation. In addition, it is worthy to note that when Ce^{4+} cations become reduced to Ce^{3+}, the isosurface of the excess spin charge density associated with the occupied gap state is incorporated with geometries, and the localized spin electrons have obvious 4f-orbital characteristics [52]. This picture is not observed neither in Fig. 6b, nor in Fig. 6c, indicating that Ce cations remained as Ce^{4+}. This lack of ability of the adsorbed hydroxyls to reoxidize the reduced surface was also observed in pure CeO_2, despite the OH species filling of the O-hole left by the oxygen removal [35].

3.3. From molecular to dissociative adsorption of water on the structural-oxygen-deficient $Ce_{0.875}Mn_{0.125}O_{1.9375}$(1 1 1) slab without a surface oxygen vacancy

Our study of dissociative adsorption of water showed that on the bare $Ce_{0.875}Mn_{0.125}O_{1.9375}$(1 1 1) surface the OH and H species preferably bonded to a Mn dopant and to an oxygen coordinated with Ce cations, respectively. Despite water could perform dissociative interactions on surface Ce cations, the calculations showed no significant difference in energy between molecular (H_2O) and dissociated (OH and H) configurations (−0.44 eV vs. −0.67 eV, for the Ce2 site), suggesting that both configurations are not far from equilibrium. However, water interaction on surface Mn dopant led to the higher energetic stability of dissociated OH and H species ($\Delta E_{ads,OH-H} = -1.21$ eV, see Table 2). Thus, we studied the process by which the H_2O molecule became dissociated into OH and H products on Mn sites.

We used the Climbing Image Nudge Elastic Band (CI-NEB) method to find the minimum energy path between the initial and final states, which correspond to molecular and dissociative adsorption of water, respectively. In the initial state (IS), the H_2O

Table 3
Bader charge, spin magnetization and estimated oxidation state of Mn cations in the different structural-oxygen-deficient $Ce_{0.875}Mn_{0.125}O_{1.9375}$(1 1 1) systems.

System	Cation	Bader charge (e)	Spin magnetization (μ_B)	Estimated oxidation state
$Ce_{0.875}Mn_{0.125}O_{1.9375}$(1 1 1) surface	Mn1	5.15	4.00	3+
	Mn2	5.15	4.16	3+
	Mn3	5.15	4.15	3+
	Mn4	5.15	4.13	3+
$Ce_{0.875}Mn_{0.125}O_{1.9375}$(1 1 1) surface with the O4-vacancy	Mn1	5.16	3.99	3+
	Mn2	5.41	4.81	2+
	Mn3	5.40	4.83	2+
	Mn4	5.15	4.13	3+
OH and H species adsorbed on the $Ce_{0.875}Mn_{0.125}O_{1.9375}$(1 1 1) surface with the O4-vacancy	Mn1	5.15	4.00	3+
	Mn2	5.39	4.81	2+
	Mn3	5.40	4.84	2+
	Mn4	5.14	4.12	3+

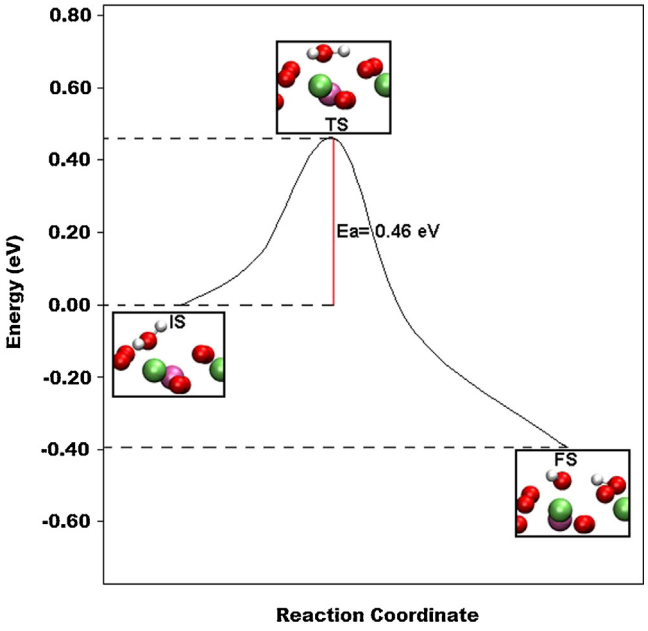

Fig. 7. Water dissociation on the $Ce_{0.875}Mn_{0.125}O_{1.9375}(1\,1\,1)$ surface. The three snapshots correspond to initial state (IS): the adsorbed H_2O molecule, transition state (TS), and final state (FS): the adsorbed OH and H species.

molecule located above the Mn dopant. In the final state (FS), the OH group bonded to the Mn cation and the H bonded to the nearest-neighbor surface O anion.

Fig. 7, shows the resulting path for water dissociation on the oxidized Mn-doped $CeO_2(1\,1\,1)$ surface. The indicated transition state (TS) is the state of maximum energy of this path and is necessary to determine the activation energy of water dissociation process. This energy barrier, i.e. $E_{[TS]} - E_{[IS]}$, resulted in 0.46 eV.

At the transition state, the distance between the hydrogen that dissociated and the O_{H_2O} was 1.03 Å, while that between this O_{H_2O} and the surface Mn dopant (the water adsorption site) was 2.04 Å. The H species that dissociated was adsorbed atop the surface O_{Ce} anion, at a distance of 1.67 Å. Considering the spin-polarized Bader charge, our calculations indicate that oxidation states of Ce and Mn cations remained unaltered after water interactions on the 12.5% Mn-doped $CeO_2(1\,1\,1)$ slab without surface O-defects, and that there were no charge transfer between H_2O molecule or OH and H species and the corresponding active sites.

Recently, it was concluded from first-principles investigations that complete dissociation of water on $CeO_2(1\,1\,1)$ surface is not favorable [25]. In this case, the calculated molecular and hydroxyl-pair structures are very close in energy with differences in the range of ~10–30 meV, depending on the exchange-correlation functional considered, and are separated by an energy barrier of ~100 meV [25]. On the other hand, our results show that Mn dopant could promote water dissociation into hydroxyls. Although this process involved an energy barrier of 0.46 eV, it would be easily overcome under realistic reaction conditions. Therefore, it is important to highlight that this characteristic of the $Ce_{0.875}Mn_{0.125}O_{1.9375}(1\,1\,1)$ surface being able to dissociate H_2O molecule, could be the key behind the high performance of MnO_x–CeO_2 catalysts in oxidation reactions, as will be considered in the Discussion section.

3.4. Surface oxygen vacancy formation on the structural-oxygen-deficient $Ce_{0.875}Mn_{0.125}O_{1.9375}(1\,1\,1)$ slab after dissociative adsorption of water over a Mn dopant

Experimental and theoretical studies have indicated that H_2O adsorption facilitated the O-vacancies formation on CeO_2 [28,33,35,38]. Besides, previous calculations of anionic vacancy formation energy indicated that Mn-doped $CeO_2(1\,1\,1)$ surface is clearly more prone to release oxygen than pure $CeO_2(1\,1\,1)$ surface [49,55]. Thus, we evaluated the formation of a surface oxygen vacancy on the $Ce_{0.875}Mn_{0.125}O_{1.9375}(1\,1\,1)$ slab with water adsorbed on it. For that purpose, we chose the most stable structure with the OH and H species adsorbed on top of Mn1 and O_{Ce}, respectively. Starting from that H—OH/$Ce_{0.875}Mn_{0.125}O_{1.9375}(1\,1\,1)$ system, we removed O4, the most easily removable surface oxygen anion, and evaluated the O4-vacancy formation energy as follows:

$$\Delta_{E_{vacO4,H-OH_{ads}}} = E_{[VacO4-(H-OH)/Ce_{0.875}Mn_{0.125}O_{1.9375}(1\,1\,1)]} + \frac{1}{2}E_{[O_2]} - E_{[(H-OH)/Ce_{0.875}Mn_{0.125}O_{1.9375}(1\,1\,1)]}$$

where $E_{[VacO4-(H-OH)/Ce_{0.875}Mn_{0.125}O_{1.9375}(1\,1\,1)]}$ and $E_{[(H-OH)/Ce_{0.875}Mn_{0.125}O_{1.9375}(1\,1\,1)]}$ represent the total energy of the HOH/$Ce_{0.875}Mn_{0.125}O_{1.9375}(1\,1\,1)$ systems with and without the surface O4-vacancy, respectively. $E_{[O_2]}$ is the calculated energy for the oxygen molecule in vacuum.

The computed O4-vacancy formation energy is $\Delta E_{vacO4,H-OH_{ads}} = 1.49$ eV. This value indicates that surface oxygen defect creation on the H—OH/$Ce_{0.875}Mn_{0.125}O_{1.9375}(1\,1\,1)$ system resulted to be less favorable than that on the bare $Ce_{0.875}Mn_{0.125}O_{1.9375}(1\,1\,1)$ surface (0.38 eV), but still more favorable than a single O-defect creation on the bare $CeO_2(1\,1\,1)$ face (2.69 eV).

3.5. Discussion

The DFT + *U* study performed in this work shows that molecular adsorptions of water on Mn and different Ce (Ce2, Ce5, Ce6 and Ce7) sites of the structural-oxygen-deficient $Ce_{0.875}Mn_{0.125}O_{1.9375}(1\,1\,1)$ slab resulted in O_{H_2O}-cation binding interactions, with one of the H_{H_2O} atoms interacting with an oxygen anion of the extra O-layer. The most favorable interaction resulted from chemisorption of the H_2O molecule on Mn dopant with a calculated adsorption energy value of -0.81 eV. Besides, our computed energy values for molecular adsorption of H_2O on Ce6 and Ce5 sites ($\Delta E_{ads,H_2O} = -0.53$ and -0.5 eV, respectively) are close to those previously reported for the most stable configuration of water on undoped $CeO_2(1\,1\,1)$ surface [23,25–32].

The most favorable dissociative interaction of water on the structural-oxygen-deficient $Ce_{0.875}Mn_{0.125}O_{1.9375}(1\,1\,1)$ slab without surface oxygen vacancies, resulted in chemisorption of the OH species on Mn dopant ($\Delta E_{ads,OH-H} = -1.21$ eV). The energy released due to this interaction is 50% higher than that of molecular adsorption on the same Mn site. The length of the formed O_{OH}–Mn bond (1.89 Å) is similar to that of Mn-O_{slab} bonds, suggesting that surface Mn cation could restore its O-coordination sphere when binding to an OH group. Considering OH species interactions on Ce cations, we note the computed configurations are significantly less stable than the structure obtained when OH chemisorbed on Mn site. Besides, the calculated O_{OH}–Ce distances from dissociated water interactions on Ce cations (in the range of 2.18–2.23 Å) were ~10% larger than those of O–Ce bonds in the slab.

On the other hand, the CI-NEB calculations showed that adsorbed H_2O molecule (over Mn dopant) needs to overcome an energy barrier of 0.46 eV in order to dissociate into OH and H fragments. We noted the whole reaction is exothermic and, thus, the energy required for those fragments to re-associate is higher than the calculated barrier for the dissociation of water molecule. Consequently, even if energy is provided to re-associate the OH and H fragments, dissociation of H_2O molecule would be faster. However, on the undoped $CeO_2(1\,1\,1)$ surface, the adsorbed hydroxyl pair

could recombine to form the H_2O molecule, and thus, it should be expected the coexistence of these two states at low temperatures [25]. Accordingly, the high catalytic performance of MnO_x–CeO_2 mixed oxides in reactions involving water, could be linked to their ability to dissociate H_2O after its molecular adsorption. Recently, it has been reported that catalytic activity of bare supports toward the WGS reaction is higher in MnO_x–CeO_2 mixed samples than in pure ceria or manganese oxide [22]. We underline the two main reaction mechanisms proposed for WGS, the regenerative redox and the associative [68], involve water dissociation. Water can dissociate on the catalyst surface to produce H_2 and refill an O-vacant site (redox mechanism), or to generate OH species, which combine with adsorbed CO to form intermediates like formate and/or carbonate (associative mechanism). Particularly, for CeO_2-based supports, it has been observed the formation of intermediate species produced by the reaction of CO with the terminal hydroxyl groups of ceria [69]. Therefore, the high catalytic activity of MnO_x–CeO_2 mixed oxides for the WGS reaction could be related to their capacity to dissociate water. Furthermore, many authors have also reported the high catalytic performance of Mn–Ce–O solid solutions toward phenol oxidation from solutions containing this pollutant [9,12,24]. In fact, it was suggested that OH plays a predominant role in the first stage of phenol adsorption-oxidation process on MnO_x–CeO_2 catalysts, resulting in a higher activity compared to that on pure CeO_2 [24]. In this way, water becoming dissociated on the substrate could lead to surface OH species that interact with phenol molecules resulting in phenol chemisorption, which is essential for the adsorbate to continue reacting.

On the other hand, the formation of O4-vacancy (O4 is the most easily removable surface oxygen) on the H—OH/$Ce_{0.875}Mn_{0.125}O_{1.9375}$(1 1 1) slab was 1.1 eV less favorable than that on the bare Mn-doped CeO_2(1 1 1) face. In a previous work, we showed that after O4 removal from the bare surface, the oxygen O12 (see oxygen labels in Fig. 2b) displaced toward the O4-hole and fills it [49]. However, when O4 was removed from the surface with adsorbed OH and H fragments on it, Mn1 bonded to O12 (see O12 location in Fig. 2b) restricting its mobility and, thus, preventing the filling of the O4-hole. Consequently, dissociative adsorption of water on Mn sites would not facilitate the creation of surface oxygen vacancies on $Ce_{0.875}Mn_{0.125}O_{1.9375}$(1 1 1), in contrast with the promoting effect observed for undoped ceria [34,35,40].

In summary, our results indicated that Mn dopant has a key role in enhancing the dissociative chemisorption of water. In this regard, we underline that CeO_2–MnO_x mixed oxides are very promising catalysts for phenol oxidation and water-gas shift reaction, for which the dissociation of water is a essential step of the reaction mechanisms [9,12,22,24].

4. Conclusions

The calculated energy values for water interactions on different sites of the 12.5% Mn-doped CeO_2(1 1 1) surface revealed that Mn is the most active site for both H_2O adsorption and hydroxyls formation. On the bare surface, H_2O molecule could adsorb over a Mn cation (-0.81 eV) forming an O-Mn bond as well as one H—$O_{surface}$ bond. On the other hand, OH and H species could chemisorb (−1.21 eV) by bonding to surface Mn and O_{Ce} ions, respectively. Besides, the calculated energy barrier for the dissociation of adsorbed water molecule into hydroxyls is 0.46 eV, which would be easily overcome under average reaction conditions.

Dissociative interaction of H_2O on the slab with a single surface oxygen vacancy is less favorable than that on the bare slab, leading to adsorption of OH species over the O-hole (left by the surface oxygen vacancy formation) and H_{H_2O} bonding to surface oxygen. In this regard, spin-polarized Bader charge calculations indicated that no reoxidation of Mn^{2+} cations occur.

Finally, we found that the vdW interactions did not modify neither the calculated adsorption energies nor the geometry of the molecularly and dissociatively adsorbed water structures on the $Ce_{0.875}Mn_{0.125}O_{1.9375}$(1 1 1) surface.

Acknowledgements

We thankfully acknowledge financial support from the Universidad de Buenos Aires (UBACyT-20020110200044), Universidad Nacional del Sur, CIC-BA, CONICET (PIP 11220090100785) and ANPCyT (PICT-2010-1770 and 2011-1312). D. García-Pintos thanks FIUBA for a Peruilh doctoral fellowship.

References

[1] J. Paier, Ch. Penschke, J. Sauer, Oxygen defects and surface chemistry of ceria: quantum chemical studies compared to experiment, Chem. Rev. 113 (6) (2013) 3949–3985.
[2] A. Trovarelli, Catalysis by Ceria and Related Materials, Imperial College Press, London, 2002.
[3] E. Aneggi, M. Boaro, C. Leitenburg, G. Dolcetti, A. Trovarelli, Insights into the redox properties of ceria-based oxides and their implications in catalysis, J. Alloys Compd. 408 (2006) 1096–1102.
[4] J. Kašpar, P. Fornasiero, M. Graziani, Use of CeO_2-based oxides in the three-way catalysis, Catal. Today 50 (1999) 285–298.
[5] C. Zhang, A. Michaelides, D. King, S. Jenkins, Oxygen vacancy clusters on ceria: decisive role of cerium f electrons, Phys. Rev. B: Condens. Matter 79 (2009) 075433(1)–075433(11).
[6] P. Dholabhai, J. Adams, P. Crozier, R. Sharma, Oxygen vacancy migration in ceria and Pr-doped ceria: a DFT+U study, J. Chem. Phys. 132 (2010) 094104(1)–094104(8).
[7] Z. Yang, Y. Wei, Z. Fu, K. Hermansson, Facilitated vacancy formation at Zr-doped ceria(1 1 1) surfaces, Surf. Sci. 602 (2008) 1199–1206.
[8] Q. Liang, X. Wu, D. Weng, H. Xu, Oxygen activation on Cu/Mn–Ce mixed oxides and the role in diesel soot oxidation, Catal. Today 139 (2008) 113–118.
[9] H. Chen, A. Sayari, A. Adnot, F. Larachi, Composition-activity effects of Mn–Ce–O composites on phenol catalytic wet oxidation, Appl. Catal., B: Environ. 32 (2001) 195–204.
[10] M. Zhang, D. Jiang, H. Jiang, Enhanced oxygen storage capacity of $Ce_{0.88}Mn_{0.12}O_y$ compared to CeO_2: an experimental and theoretical investigation, Mater. Res. Bull. 47 (2012) 4006–4012.
[11] W. Hong, S. Iwamoto, S. Hosokawa, K. Wada, H. Kanai, M. Inoue, Effect of Mn content on physical properties of CeO_x–MnO_y support and BaO–CeO_x–MnO_y catalysts for direct NO decomposition, J. Catal. 277 (2011) 208–216.
[12] D. Delimaris, T. Ioannides, VOC oxidation over MnO_x–CeO_2 catalysts prepared by a combustion method, Appl. Catal., B: Environ. 84 (2008) 303–312.
[13] W. Shan, N. Ma, J. Yang, X. Dong, C. Liu, L. Wei, Catalytic oxidation of soot particulates over MnO_x–CeO_2 oxides prepared by complexation–combustion method, J. Nat. Gas Chem. 19 (2010) 86–90.
[14] M. Abecassis-Wolfovich, R. Jothiramalingam, M. Landau, M. Herskowitz, B. Viswanathan, T. Varadarajan, Cerium incorporated ordered manganese oxide OMS-2 materials: improved catalysts for wet oxidation of phenol compounds, Appl. Catal., B: Environ. 59 (2005) 91–98.
[15] L. Shi, W. Chu, F. Qu, S. Luo, Low-temperature catalytic combustion of methane over MnO_x–CeO_2 mixed oxide catalysts: effect of preparation method, Catal. Lett. 113 (1) (2007) 59–64.
[16] X. Tang, Y. Li, X. Huang, Y. Xu, H. Zhu, J. Wang, W. Shen, MnO_x–CeO_2 mixed oxide catalysts for complete oxidation of formaldehyde: effect of preparation method and calcination temperature, Appl. Catal., B: Environ. 62 (2006) 265–273.
[17] G. Zhou, P. Shah, R. Gorte, A study of cerium–manganese mixed oxides for oxidation catalysis, Catal. Lett. 120 (3) (2008) 191–197.
[18] Y. Tu, M. Meng, Zh. Sun, L. Zhang, T. Ding, T. Zhang, CO preferential oxidation over Au/MnO_x–CeO_2 catalysts prepared with ultrasonic assistance: effect of calcination temperature, Fuel Process. Technol. 93 (2012) 78–84.
[19] Q. Guo, Y. Liu, MnO_x modified Co_3O_4–CeO_2 catalysts for the preferential oxidation of CO in H_2-rich gases, Appl. Catal., B: Environ. 82 (2008) 19–26.
[20] L. Jiang, B. Ye, K. Wei, Effects of CeO_2 on structure and properties of Ni–Mn–K/bauxite catalysts for water–gas shift reaction, J. Rare Earths 26 (2008) 352–356.
[21] X. Du, Z. Yuan, L. Cao, Ch. Zhang, Sh. Wang, Water gas shift reaction over Cu–Mn mixed oxides catalysts: effects of the third metal, Fuel Process. Technol. 89 (2008) 131–138.
[22] E. Poggio Fraccari, O. D'Alessandro, J. Sambeth, G. Baronetti, F. Mariño, Ce–Mn mixed oxides as supports of copper- and nickel-based catalysts for water–gas shift reaction, Fuel Process. Technol. 119 (2014) 67–73.
[23] M. Molinari, S. Parker, D. Sayle, M. Islam, Water adsorption and its effect on the stability of low index stoichiometric and reduced surfaces of ceria, J. Phys. Chem. C 116 (2012) 7073–7082.

[24] O. DíAlessandro, H. Thomas, J. Sambeth, An analysis of the first steps of phenol adsorption–oxidation over coprecipitated Mn–Ce catalysts: a DRIFTS study, React. Kinet. Mech. Cat. 107 (2012) 295–309.
[25] D. Fernández-Torre, K. Kósmider, J. Carrasco, M.V. Ganduglia-Pirovano, R. Pérez, Insight into the adsorption of water on the clean CeO_2(1 1 1) surface with van der Waals and hybrid density functionals, J. Phys. Chem. C 116 (2012) 13584–13593.
[26] S. Kumar, P. Schelling, Density functional theory study of water adsorption at reduced and stoichiometric ceria(1 1 1) surfaces, J. Chem. Phys. 125 (2006) 204704(1)–204704(8).
[27] M. Watkins, A. Foster, A. Shluger, Hydrogen cycle on CeO_2(1 1 1) surfaces: density functional theory calculations, J. Phys. Chem. C 111 (2011) 15337–15341.
[28] M. Fronzi, S. Piccinin, B. Delley, E. Traversa, C. Stampfl, Water adsorption on the stoichiometric and reduced CeO_2(1 1 1) surface: a first-principles investigation, Phys. Chem. Chem. Phys. 11 (2009) 9188–9199.
[29] D. Marrocchelli, D. Yildiz, First-principles assessment of H_2S and H_2O reaction mechanisms and the subsequent hydrogen absorption on the CeO_2(1 1 1) surface, J. Phys. Chem. C 116 (2012) 2411–2424.
[30] Z. Yang, Q. Wang, S. Wei, The synergistic effects of the Cu–CeO_2(1 1 1) catalysts on the adsorption and dissociation of water molecules, Phys. Chem. Chem. Phys. 13 (2011) 9363–9373.
[31] H.-T. Chen, Y. Choi, M. Liu, M. Lin, A theoretical study of surface reduction mechanisms of CeO_2(1 1 1) and (1 1 0) by H_2, Chem. Phys. Chem. 8 (2007) 849–855.
[32] S. Fuente, M. Branda, F. Illas, Role of step sites on water dissociation on stoichiometric ceria surfaces, Theor. Chem. Acc. 131 (2012) 1190(1)–1190(7).
[33] Z. Yang, Q. Wang, S. Wei, D. Ma, Q. Sun, The effect of environment on the reaction of water on the ceria(1 1 1) surface: a DFT + *U* study, J. Phys. Chem. C 114 (2010) 14891–14899.
[34] S. Gritschneder, Y. Iwasawa, M. Reichling, Strong adhesion of water to CeO_2(1 1 1), Nanotechnology 18 (2007) 044025 (1)–044025 (6).
[35] M. Henderson, C. Perkins, M. Engelhard, S. Thevuthasan, C. Peden, Redox properties of water on the oxidized and reduced surfaces of CeO_2(1 1 1), Surf. Sci. 526 (2003) 1–18.
[36] L. Kundakovic, D. Mullins, S. Overbury, Adsorption and reaction of H_2O and CO on oxidized and reduced Rh/CeO_x(1 1 1) surfaces, Surf. Sci. 457 (2000) 51–62.
[37] X. Zhao, S. Ma, J. Hrbek, J. Rodriguez, Reaction of water with Ce–Au(1 1 1) and CeO_x/Au(1 1 1) surfaces: photoemission and STM studies, Surf. Sci. 601 (2007) 2445–2452.
[38] V. Matolín, I. Matolínova, F. Dvorak, V. Johanek, J. Myslivecek, K. Prince, T. Skala, O. Stetsovych, N. Tsud, M. Vaclavu, B. Smíd, Water interaction with CeO_2(1 1 1)/Cu(1 1 1) model catalyst surface, Catal. Today 181 (2012) 124–132.
[39] Y. Lykhach, V. Johánek, H. Aleksandrov, S. Kozlov, M. Happel, T. Skála, P. St Petkov, N. Tsud, G. Vayssilov, K. Prince, K. Neyman, V. Matolín, J. Libuda, Water chemistry on model ceria and Pt/ceria catalysts, J. Phys. Chem. C 116 (2012) 12103–12113.
[40] D. Mullins, P. Albrecht, T.-L. Chen, F. Calaza, M. Biegalski, H. Christen, S. Overbury, Water dissociation on CeO_2(1 0 0) and CeO_2(1 1 1) thin films, J. Phys. Chem. C 116 (2012) 19419–19428.
[41] G. Kresse, J. Furthmuller, Efficiency of ab-initio total energy calculations for metals and semiconductors using a plane-wave basis set, Comput. Mater. Sci. 6 (1996) 15–50.
[42] G. Kresse, J. Hafner, Ab initio molecular dynamics for liquid metals, Phys. Rev. B: Condens. Matter 47 (1997) 558–561.
[43] J. Perdew, K. Burke, M. Ernzerhof, Generalized gradient approximation made simple, Phys. Rev. Lett. 77 (1996) 3865–3868.
[44] G. Kresse, D. Joubert, From ultrasoft pseudopotentials to the projector augmented-wave method, Phys. Rev. B: Condens. Matter 59 (1999) 1758–1775.
[45] H. Monkhorst, J. Pack, Special points for Brillouin-zone integrations, Phys. Rev. B: Condens. Matter 13 (1976) 5188–5192.
[46] S. Dudarev, G. Botton, S. Savrasov, C. Humphreys, A. Sutton, Electron-energy-loss spectra and the structural stability of nickel oxide: an LSDA + *U* study, Phys. Rev. B: Condens. Matter 57 (1998) 1505–1509.
[47] V. Anisimov, J. Zaanen, O. Andersen, Band theory and Mott insulators: Hubbard *U* instead of Stoner I, Phys. Rev. B: Condens. Matter 44 (1991) 943–954.
[48] J. Klimes, D. Bowler, A. Michaelides, Van der, Waals density functionals applied to solids, Phys. Rev. B: Condens. Matter 83 (2011) 195131(1)–195131(13).
[49] D. García Pintos, A. Juan, B. Irigoyen, Mn-doped CeO_2: DFT + *U* study of a catalyst for oxidation reactions, J. Phys. Chem. C 117 (2013) 18063–18073.
[50] M. Nolan, S. Grigoleit, D. Sayle, S. Parker, G. Watson, Density functional theory studies of the structure and electronic structure of pure and defective low index surfaces of ceria, Surf. Sci. 576 (2005) 217–229.
[51] M. Nolan, J. Fearon, G. Watson, Oxygen vacancy formation and migration in ceria, Solid State Ionics 177 (2006) 3069–3074.
[52] H. Li, H. Wang, X. Gong, Y. Guo, G. Lu, P. Hu, Multiple configurations of the two excess 4f electrons on defective CeO_2(1 1 1): origin and implications, Phys. Rev. B: Condens. Matter 79 (2009) 193401(1)–193401(4).
[53] C. Castleton, J. Kullgren, K. Hermansson, Tuning LDA + *U* for electron localization and structure at oxygen vacancies in ceria, J. Chem. Phys. 127 (2007) 244704(1)–244704(11).
[54] M. Nolan, S. Parker, G. Watson, The electronic structure of oxygen vacancy defects at the low index surfaces of ceria, Surf. Sci. 595 (2005) 223–232.
[55] W. Cen, Y. Liu, Z. Wu, H. Wang, X. Weng, A theoretic insight into the catalytic activity promotion of CeO_2 surfaces by Mn doping, Phys. Chem. Chem. Phys. 14 (2012) 5769–5777.
[56] Y. Tang, H. Zhang, L. Cui, C. Ouyang, S. Shi, W. Tang, H. Li, J. Lee, L. Chen, First-principles investigation on redox properties of M-doped CeO_2(M = Mn,Pr,Sn,Zr), Phys. Rev. B: Condens. Matter 82 (2010) 125104(1)–125104(9).
[57] Ch. Kang, H. Kusaba, H. Yahiro, K. Sasaki, Y. Teraoka, Preparation, characterization and electrical property of Mn-doped ceria-based oxides, Solid State Ionics 177 (2006) 1799–1802.
[58] A. Gupta, U.V. Waghmare, M.S. Hegde, Correlation of oxygen storage capacity and structural distortion in transition-metal-, noble-metal-, and rare-earth-ion-substituted CeO_2 from first principles calculation, Chem. Mater. 22 (2010) 5184–5198.
[59] M. Branda, R. Ferullo, M. Causà, Francesc Illas, relative stabilities of low index and stepped CeO_2 surfaces from hybrid and GGA + *U* implementations of density functional theory, J. Phys. Chem. C 115 (2011) 3716–3721.
[60] A. Siokou, R.M. Nix, Interaction of methanol with well-defined ceria surfaces: reflection/absorption infrared spectroscopy, X-ray photoelectron spectroscopy, and temperature-programmed desorption study, J. Phys. Chem. B 103 (1999) 6984–6997.
[61] Y. Namai, K.-i. Fukui, Y. Iwasawa, Atom-resolved noncontact atomic force microscopic observations of CeO_2(1 1 1) surfaces with different oxidation states: surface structure and behavior of surface oxygen atoms, J. Phys. Chem. B 107 (2003) 11666–11673.
[62] M. Fronzi, A. Soon, B. Delley, E. Traversa, C. Stampfl, Stability and morphology of cerium oxide surfaces in an oxidizing environment: a first-principles investigation, J. Chem. Phys. 131 (2009) 104701(1)–104701(16).
[63] Z. Yang, T. Woo, M. Baudin, K. Hermansson, Atomic and electronic structure of unreduced and reduced CeO2 surfaces: a first-principles study, J. Chem. Phys. 120 (2004) 7741–7749.
[64] G. Henkelman, A. Arnaldsson, H. Jónsson, A fast and robust algorithm for Bader decomposition of charge density, Comput. Mater. Sci. 36 (2006) 354–360.
[65] B. Herschend, M. Baudin, K. Hermansson, Electronic structure of the CeO_2(1 1 0) surface oxygen vacancy, Surf. Sci. 599 (2005) 173–186.
[66] B. Hwang, Y. Tsai, D. Carlier, G. Ceder, A combined computational/experimental study on $LiNi_{1/3}Co_{1/3}Mn_{1/3}O_2$, Chem. Mater. 15 (2003) 3676–3686.
[67] S. Grimme, Semiempirical GGA-type density functional constructed with a long-range dispersion correction, J. Compd. Chem. 27 (2006) 1787–1799.
[68] D.L. Trimm, Minimisation of carbon monoxide in a hydrogen stream for fuel cell application, Appl. Catal., A: Gen. 296 (2005) 1–11.
[69] T. Shido, Y. Iwasawa, Reactant-promoted reaction mechanism for water–gas shift reaction on Rh-doped CeO_2, J. Catal. 141 (1) (1993) 71–81.